Inorganic Chemistry

Article

pubs.acs.org/IC

Cluster Chemistry in Electron-Poor Ae−Pt−Cd Systems (Ae = Ca, Sr, Ba): (Sr,Ba)Pt_2Cd_4, $Ca_6Pt_8Cd_{16}$, and Its Known Antitype $Er_6Pd_{16}Sb_8$

Saroj L. Samal, Fakhili Gulo,† and John D. Corbett*

Ames Laboratory, DOE and Department of Chemistry, Iowa State University, Ames, Iowa 50010, United States

Supporting Information

ABSTRACT: Three new ternary polar intermetallic compounds, cubic $Ca_6Pt_8Cd_{16}$, and tetragonal (Sr, Ba)Pt_2Cd_4 have been discovered during explorations of the Ae−Pt−Cd systems. Cubic $Ca_6Pt_8Cd_{16}$ (*Fm*-3*m*, Z = 4, a = 13.513(1) Å) contains a 3D array of separate Cd_8 tetrahedral stars (*TS*) that are both face capped along the axes and diagonally bridged by Pt atoms to generate the 3D anionic network $Cd_8[Pt(1)]_{6/2}[Pt(2)]_{4/8}$. The complementary cationic surface of the cell consists of a face-centered cube of Pt(3)@Ca_6 octahedra. This structure is an ordered ternary variant of $Sc_{11}Ir_4$ ($Sc_6Ir_8Sc_{16}$), a stuffed version of the close relative $Na_6Au_7Cd_{16}$, and a network inverse of the recent $Er_6Sb_8Pd_{16}$ (compare $Ca_6Pt_8Cd_{16}$). The three groups of elements each occur in only one structural version. The new $AePt_2Cd_4$, Ae = Sr, Ba, are tetragonal ($P4_2/mnm$, Z = 2, $a \approx 8.30$ Å, $c \approx 4.47$ Å) and contain chains of edge-sharing Cd_4 tetrahedra along c that are bridged by four-bonded Ba/Sr. LMTO-ASA and ICOHP calculation results and comparisons show that the major bonding (Hamilton) populations in $Ca_6Pt_8Cd_{16}$ and $Er_6Sb_8Pd_{16}$ come from polar Pt−Cd and Pd−Sb interactions, that Pt exhibits larger relativistic contributions than Pd, that characteristic size and orbital differences are most evident for Sb 5s, Pt_8, and Pd_{16}, and that some terms remain incomparable, Ca−Cd versus Er−Pd.

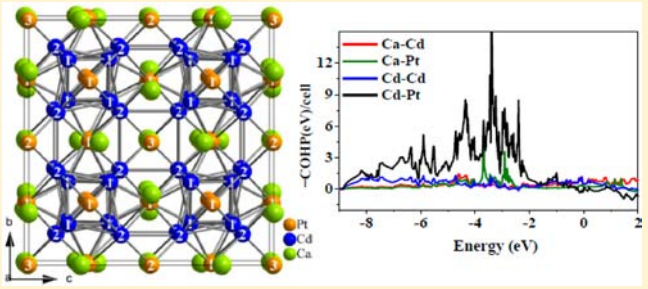

INTRODUCTION

Exploratory syntheses have played significant roles in solid-state and materials chemistry in the discovery of new compounds and the revelation of their chemical and physical properties. The heavy group 13 elements (triels) yield several novel binary polyanionic cluster compounds in which alkali (A) or alkaline-earth metals (Ae) act as electropositive counterions.[1,2] Additions of a third late transition metal to the systems, gold, in particular, have led to major gains in terms of new structures and bonding patterns and enhanced bonding. Several gold-based ternary compounds with fascinating structures and unusual bonding pattern have been discovered in A/Ae−Au−Tr/Di systems (Tr = Ga, In; Di = Zn, Cd).[3−15] For example, we recently isolated $Na_6Au_7Cd_{16}$ which contains tetrahedral star clusters of cadmium,[13] and several ternary compounds in K/Rb−Au−In systems with intriguing tunnel structures.[5,6] The Na−Au−Zn system contains two new compounds with linear tunnels that are populated by new examples of somewhat diffuse but locally ordered Na cation distributions.[14] Switches to more tightly bound Ae metals generally produce substantial changes in products, particularly with higher symmetry and more uniform packing. Thus, the ternary $BaAu_xZn_{13-x}$ system ($1< x < 8$) contains a broad substitution derivative of cubic $BaZn_{13}$ as well as a closely related tetragonal phase.[15]

Relatively few studies have been carried out on the neighboring platinum-based ternary intermetallic systems,[16−23] although some amount of gold's relativistically enhanced bonding properties[24] would seem likely for Pt as well. The latter yields a 3D [$PtIn_2$] network in $CaPtIn_2$[16] with Ca in distorted pentagonal channels, whereas Ca_2Pt_2Cd[17] and Ca_2Pt_2In[18] feature planar [Pt_2Cd] and [Pt_2In] networks. The compound $Ca_6Pt_{2.33}Zn_{5.67}$ contains puckered networks of Pt and Zn.[21] The rare-earth-metal (R) rich $La_{23}Pt_7Cd_4$[22] and Gd_4PtCd[23] contain transition-metal-centered trigonal prisms of rare-earth-metal atoms and isolated cadmium tetrahedra. Here we report the synthesis, structure, and bonding of two new compound types, $Ca_6Pt_8Cd_{16}$, a close relative of the unusual $Na_6Au_7Cd_{16}$[13] and (Sr/Ba)Pt_2Cd_4 which contain Cd tetrahedral stars in a closely knit cubic structure and chains of condensed cadmium tetrahedra, respectively. The report of $Er_6Pd_{16}Sb_8$ in the recent literature,[25] an antitype relative of the present network in$Ca_6Pt_8Cd_{16}$, raises more interesting questions about relationships between similar but reordered elements in this relatively unusual structure type.

EXPERIMENTAL SECTION

Syntheses. The starting materials dendritic calcium, strontium, barium (99.9%), and cadmium (99.999%, all from Alfa Aesar) and platinum (99.995%, from Lonmin) were handled in dry N_2 (≤0.1 ppm H_2O by volume). The weighed reactants were weld sealed in tantalum containers and subsequently enclosed in an evacuated silica jacket to protect Ta from air when heated. A series of Ae−Pt−Cd compositions was reacted at 950 °C for 12 h, quenched in cold water, and annealed at 650 °C for 4 days. Crystals of $Ca_6Pt_8Cd_{16}$ were initially picked from

Received: December 17, 2012
Published: February 18, 2013

   dx.doi.org/10.1021/ic302767b | *Inorg. Chem.* 2013, 52, 2697−2704

Table 1. Crystal Data and Structure Refinement Parameters for $Ca_6Pt_8Cd_{16}$, $BaPt_2Cd_4$, and $SrPt_2Cd_4$

empirical formula	$Ca_6Pt_8Cd_{16}$	$BaPt_2Cd_4$	$SrPt_2Cd_4$
fw	1799.80	977.12	927.42
space group, Z	Fm-3m, 4	$P4_2/mnm$, 2	$P4_2/mnm$, 2
unit cell dimensions	a = 13.5101(16) Å	a = 8.372(2) Å, c = 4.4624(9) Å	a = 8.235(1) Å, c = 4.4817(9) Å
vol., Å^3	2465.9(5)	312.76(9)	303.93(9)
density (calcd), Mg/m^3	9.696	10.37	10.13
abs coeff, mm^{-1}	59.860	63.93	68.12
theta range for data collection, deg	2.61−28.26	3.44−28.27	3.50−28.26
index ranges	$-17 \le h \le 17$, $-17 \le k \le 18$, $-17 \le l \le 17$	$-10 \le h \le 10$, $-11 \le k \le 11$, $-5 \le l \le 5$	$-10 \le h \le 10$, $-10 \le k \le 10$, $-5 \le l \le 5$
no. of reflns collected	5429	2540	2453
no. of indep. obsd reflns	196 (R_{int} = 0.0473)	234 (R_{int} = 0.0359)	230 (R_{int} = 0.0421)
data completeness	0.990	0.987	0.981
data/restraints/parameters	196/0/16	234/0/15	230/0/15
goodness-of-fit on F^2	1.107	1.138	1.188
final R_1, wR_2 [$I > 2\sigma(I)$]	0.0183, 0.0425	0.0173, 0.0347	0.0200, 0.0405
final R_1, wR_2 (all data)	0.0189, 0.0426	0.0185, 0.0349	0.0213, 0.0408
largest diff. peak and hole, e·Å^{-3}	1.66,−2.41	1.07,−1.06	1.47,−2.03

[a] $R=\Sigma||F_o| - |F_c||/\Sigma|F_o|$; $R_w = [\Sigma w(|F_o| - |F_c|)^2/\Sigma w(F_o)^2]^{1/2}$; $w = 1/\sigma_F^2$

a $CaPt_2Cd_4$ composition. Later, ∼90% pure phase was synthesized from the refined stoichiometry after different annealing temperatures were investigated. The product of an 850 °C annealing was primarily $CaPtCd_2$[26] instead, but the target phase was obtained in increasing yields following annealing at 650 and 550 °C for 6 days. The best yield, ∼90%, resulted after 10 days at 500 °C. An increasing amount of $CaPtCd_2$ appears after 6 days at increasing temperatures up to 850 °C, suggesting some unseen loss of Pt or Cd values with temperature.

The composition and structure of the inverse $Er_6Pd_{16}Sb_8$[25] were also confirmed. An effectively single-phase product (Figure S2, Supporting Information) was obtained after prereaction of a 2:1 molar mixture of Pd and Sb at 900 °C in Ta to give Pd_2Sb,[27] brief arc melting of this with stoichiometric Er, and then their equilibration in a sealed Ta/SiO_2 dual container at 700 °C for 3 days. This contrasts with the mixtures obtained earlier[25] after arc melting of a mixture of the prescribed proportions of all three elements followed by equilibration in alumina for 10−15 days at 700 °C.

Attempts to synthesize the Sr and Ba analogues of $Ca_6Pt_8Cd_{16}$ led to the new tetragonal (Sr,Ba)Pt_2Cd_4 isotypes instead. Comparisons of the observed powder patterns for both products with those calculated according to the structural refinements in Figure S1, Supporting Information, attest to their high purities. All of the compounds are brittle, with metallic luster, and visually inert to air at room temperature for at least 1 h. The title compounds are evidently all close to line phases as lattice constant variations of only <3σ could be induced by compositional variations during syntheses.

X-ray Diffraction Studies. Powder diffraction data were collected at room temperature with the aid of a Stoe Stadi P powder diffractometer equipped with an image plate and Cu Kα radiation (λ = 1.54059 Å). Samples were dispersed between acetate films with the aid of a little grease and held in a Stoe airtight sample holder with a metal cover seated by screws. Lattice parameters were refined using the WinXPow program,[28] and these values were used in distance calculations from single-crystal data.

Diffraction data were collected at room temperature with the aid of a Bruker SMART CCD diffractometer equipped with Mo Kα radiation (λ = 0.71073 Å) over 2θ ranges = ∼3−57° as three sets of 606 frames with 0.3° scans in ω and exposures of 10 s per frame. The reflection intensities were integrated with the SAINT program in the SMART software package.[29] Empirical absorption corrections were made with the aid of the SADABS program.[30] Space group determinations were done with the aid of XPREP and SHELXTL 6.1.[31] Structures were solved by direct methods and subsequently refined on $|F^2|$ with combinations of least-squares refinements and difference Fourier maps.

$Ca_6Pt_8Cd_{16}$ diffraction data indicated an F-centered cubic lattice, and the structure was solved and refined in Fm-3m with six atom positions. The larger final isotropic value for Pt3 compared with Pt1 and Pt2 (0.028 versus 0.013 Å^2) and a spherical anisotropic distribution evidently arose because of fewer neighboring Ca atoms (6) and no Pt bonding. Neither atom mixing nor a partial occupancy gave a suitable alternate explanation. The final anisotropic refinement converged at R_1 = 0.0183 [$I > 2\sigma(I)$], wR_2 = 0.0425 for all data, with a goodness-of-fit on F^2 of 1.107. The structure of $BaCd_4Pt_2$ was solved in tetragonal $P4_2/mnm$ with three atom positions. The final anisotropic refinement converged at R_1 = 0.0185, wR_2 = 0.0349 for a goodness of fit F^2 = 1.138. Details regarding data collection, crystal data, and structure refinements are summarized in Table 1, and atom positions and equivalent isotropic displacement parameters for $Ca_6Pt_8Cd_{16}$ and the pair $SrCd_4Pt_2$, and $BaCd_4Pt_2$ are given in Tables 2 and 3, respectively. Anisotropic atom displacement parameters and cif data are contained in the Supporting Information.

Table 2. Atomic Coordinates and Equivalent Isotropic Displacement Parameters (Å^2) for $Ca_6Pt_8Cd_{16}$[a]

atom	Wyckoff position	x	y	z	U_{eq}
Cd1	32f	0.1651(1)	0.1651(1)	0.1651(1)	0.014(1)
Cd2	32f	0.3801(1)	0.3801(1)	0.3801(1)	0.012(1)
Ca	24e	0.2125(2)	0	0	0.015(1)
Pt1	24d	0	0.25	0.25	0.012(1)
Pt2	4b	0.5	0.5	0.5	0.013(1)
Pt3	4a	0	0	0	0.028(1)

[a] Origin at 0 0 0.

Electronic Structure Calculations. Tight binding calculations on $Ca_6Cd_{16}Pt_8$ and $BaCd_4Pt_2$ were performed according to the linear muffin-tin orbital (LMTO) method in the atomic sphere approximation (ASA).[32] The radii of the Wigner Seitz spheres were assigned automatically, so that the overlapping potentials would be the best possible approximations to the full potentials, subject to an 18% overlap restriction for atom-centered spheres.[33] No additional empty spheres were needed. Basis sets of Ca 4s, 3d, (4p), Ba 6s, 5d, (6p), Cd 5s, 5p, (4f), and Pt 6s, 6p, 5d, (5f) (downfolded orbitals in parentheses) were employed, and reciprocal space integrations were carried out using the tetrahedron method. Scalar relativistic corrections were included, which are particularly important for Pt. For bonding analysis, the energy contributions of all filled electronic states for

dx.doi.org/10.1021/ic302767b | Inorg. Chem. 2013, 52, 2697−2704

Table 3. Atomic Coordinates and Equivalent Isotropic Displacement Parameters (Å^2) for $AePt_2Cd_4$

compound	atom	Wyckoff position	site symmetry	x	y	z	U_{eq}
$BaCd_4Pt_2$	Ba	2*a*	*m.mm*	0	0	0	0.011(1)
	Pt	4*f*	*m.2m*	0.2776(1)	0.2776(1)	0	0.011(1)
	Cd	8*i*	*m..*	0.8435(1)	0.4097(1)	0	0.011(1)
$SrCd_4Pt_2$	Sr	2*a*	*m.mm*	0	0	0	0.017(1)
	Pt	4*f*	*m.2m*	0.2794(1)	0.2794(1)	0	0.016(1)
	Cd	8*i*	*m..*	0.8440(1)	0.4072(1)	0	0.015(1)

selected atom pairs were calculated by the crystal orbital Hamilton population method (COHP),[34] from which their weighted integrations up to E_F provided −ICOHP data; Hamilton populations are approximations of relative bond orders.

RESULTS AND DISCUSSION

Structural Descriptions. *$Ca_6Pt_8Cd_{16}$.* This new ternary intermetallic compound, isolated from the cadmium-rich portion of the Ca−Pt−Cd system following solid-state reactions at high temperature, crystallizes in the cubic *Fm*-3*m* space group with a = 13.510(2) Å. Cd_8 tetrahedral stars are the characteristic building blocks, Figure 1. The phase is an ordered

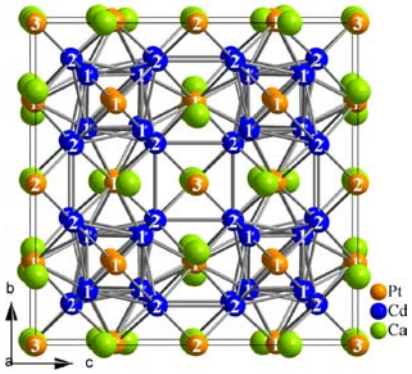

Figure 1. Structure of $Ca_6Pt_8Cd_{16}$ as constructed from Cd_8 TS (blue), each of which consists of inner Cd1 tetrahedra face capped by larger Cd2 tetrahedra. *TS* are each further face capped by six bridging Pt1 atoms (orange) and corner bridged by six Pt2 atoms in cubes between them. Role of the single type of Ca atoms (green) is described below.

ternary variant of $Sc_{11}Ir_4$[35] and a fully occupied ternary variant of binary Th_6Mn_{23},[36] the oldest member of a family of close relatives that have 4*a* or 4*b* site vacancies, as in the recently reported $Na_6Au_7Cd_{16}$[13] and its older relative $Mg_6Cu_7Si_{16}$.[37] These are still only a small part of an extensive family of tetrahedral star (TS) structures, which are often encountered in intermetallics, particularly among electron-poorer compounds (vec = 2.1−2.6 e/atom).[38,39] The present $Ca_6Pt_8Cd_{16}$ and other family members differ distinctly from the interesting $Er_6Sb_8Pd_{16}$ (nee $Er_3Pd_8Sb_4$[25]) in the clear role reversal between the late-transition- and post-transition-metal components, that is, Pt_8Cd_{16} versus Sb_8Pd_{16} in the principal cluster network. (Doubled formulas for $Er_3Pd_8Sb_4$ and $Sc_{11}Ir_4$ arise when the six Wyckoff sites are counted conventionally.)

Figure 1 shows the ~001 view of $Ca_6Pt_8Cd_{16}$ starting with the eight Cd_8 tetrahedral stars (blue), each of which consists of a pair of opposed tetrahedra with a common center point (*D*2*d* symmetry) that is centered in the octants (±1/4,1/4,1/4). The two tetrahedra that define them naturally have dissimilar edges, (d(Cd1−Cd1) = 3.24 Å and d(Cd2−Cd2) = 4.971 Å), and each of the Cd atoms in the outer tetrahedron caps a face of inner tetrahedron d(Cd1−Cd2) = 3.031 Å. The TS are each face capped by six Pt1 (yellow, *m.mm*) atoms that each bridge quadrilateral faces on six pairs of *TS* along the cell directions, as seen better in Figure 2a without the surface atoms. Parallel *TS*

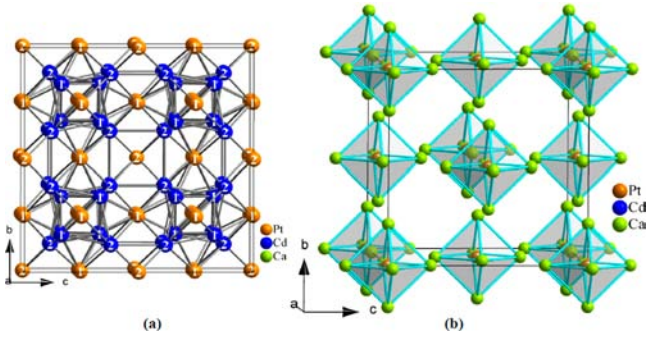

Figure 2. (a) Anionic Pt−Cd framework $Cd_8[Pt(1)]_{6/2}[Pt(2)]_{4/8}$ in $Ca_6Cd_{16}Pt_8$. Roles of Pt(1) and Pt(2) atoms in bridging between the Cd_8 TSs (blue) are as described in Figure 1. (b) Cationic face-centered-cubic sheath of Pt(3)@Ca_6 octahedra about a completes the structure of $Ca_6Pt_8Cd_{16}$.

are also directly interbonded at Cd2 (d(Cd2−Cd2) = 3.242 Å) along axial directions. Finally, the *TS* are further bridged at their Cd2 corners by relatively more distant Pt2 (*m*-3*m*) atoms, which lie on the cell center and on the cell edges. These platinum and cadmium atoms define an infinite $[Cd_8(Pt1)_{6/2}(Pt2)_{4/8}]_2$ network, which for distinction can be described as the more anionic (electronegative) part of the structure.

The remainder of the structural building blocks consist of a face-centered cube of four (net) Ca_6 octahedra per cell, each of which is centered by an otherwise isolated Pt3 atom at 0,0,0 and on the face centers of the cell (1/2 1/2 0, etc.), Figure 2b. These bond to and enclose the Cd−Pt cores described in Figure 2a and provide all of the Ca members (green spheres) that appear in Figure 1 but are not otherwise described. The Ca−Pt3 bonds (2.871(1) Å) are particularly short, befitting the smaller number of Ca about each and properly comparable to those in Ca_6PtCd_{11} (2.897(2) Å).[40]

Individual interatomic distances in $Ca_6Pt_8Cd_{16}$ are summarized in Table S3, Supporting Information. The Cd−Cd distances range from 3.031 to 3.242 Å, which are a little smaller than d(Cd−Cd) = 3.078−3.303 Å in the closely related $Na_6Au_7Cd_{16}$ which has a lower field cation. Cd−Cd distances in the condensed chains of tetrahedra in $BaPt_2Cd_4$ (below) are similar, 3.00−3.09 Å. Calcium atoms are surrounded by 13 neighbors, four Cd1, four Cd2, four Pt1, and one Pt3 (Figure S3, Supporting Information). Ca−Cd distances are effectively invariant, from 3.219 (1) to 3.221(2) Å, whereas d(Ca−Pt) vary from 2.87 to 3.42 Å in three different roles (Figure 1, Table 5). Pt3 has a simple octahedral environment of Ca, Pt2

dx.doi.org/10.1021/ic302767b | Inorg. Chem. 2013, 52, 2697−2704

has cubic cadmium neighbors, whereas Pt1 has 12 neighbors: four Cd1, four Cd2, and four Ca atoms at the vertices of a distorted icosahedron. Pt−Cd distances range over 2.758(1)−2.967(1) Å, paralleling the coordination numbers. Cd1 atoms are icosahedrally surrounded by three Ca, three Cd1, three Cd2, and three Pt1 atoms, whereas Cd2 is closely bonded to three Ca, three Cd1, three Cd2, three Pt1, and one Pt3.

The structure of ternary $Ca_6Pt_8Cd_{16}$ is described by the same Wyckoff positions and similar coordinates as the novel $Na_6Au_7Cd_{16}$,[13] except for one more Pt at (0 0 0), in the centers of the sheath of Ca octahedra in Figure 2b. Thus, $Ca_6Pt_8Cd_{16}$ is the simple filled variant of $Na_6Au_7Cd_{16}$, the gain of the set of strongly bonded Pt1@Ca6 octahedra relative to the empty Na_6 octahedra obviously being important (more discussion later). We could not obtain the counter possibilities, $Ca_6Cd_{16}Pt_7$, $Ca_6Cd_{16}Au_8$, or the inverted $Ca_6Cd_8Pt_{16}$.

$BaPt_2Cd_4$ and $SrPt_2Cd_4$. Figure 3 presents the ∼001 view of the representative tetragonal $BaPt_2Cd_4$ structure ($P4_2/mnm$), which is isostructural with $ZrFe_4Si_2$.[41] The earlier but more electronegative Pt occupies the Si position, and Cd is on the Fe site, with Ba and Zr the formal cations, relatively speaking. The basic building blocks are Cd_4 tetrahedra condensed by edge-sharing along c to form chains (Figure 3b), the side edges of each pair being bridged by a Pt atom. (The structure may also be less usefully described as alternating planar six-membered Pt_2/Cd_4 rings stacked along the c axis.) The Cd−Cd distances in the slightly distorted tetrahedra are 3.024(1) and 3.092(1) Å with unbridged edges of 2.997(1) Å. The edge-shared and Pt-bridged Cd_4 tetrahedra define cavities for the Ba or Sr atoms which occupy special (2*a*) positions and have 18 nearest neighbors: 12 Cd and 6 Pt, as shown in Figure S4, Supporting Information. Ba−Pt distances range from 3.29 to 3.45 Å, whereas the more frequent Ba−Cd values vary only slightly, from 3.671 to 3.717(1) Å. Pt−Cd distances range from 2.782 to 2.807 Å, comparable to 2.758−2.967 Å in $Ca_6Pt_8Cd_{16}$.

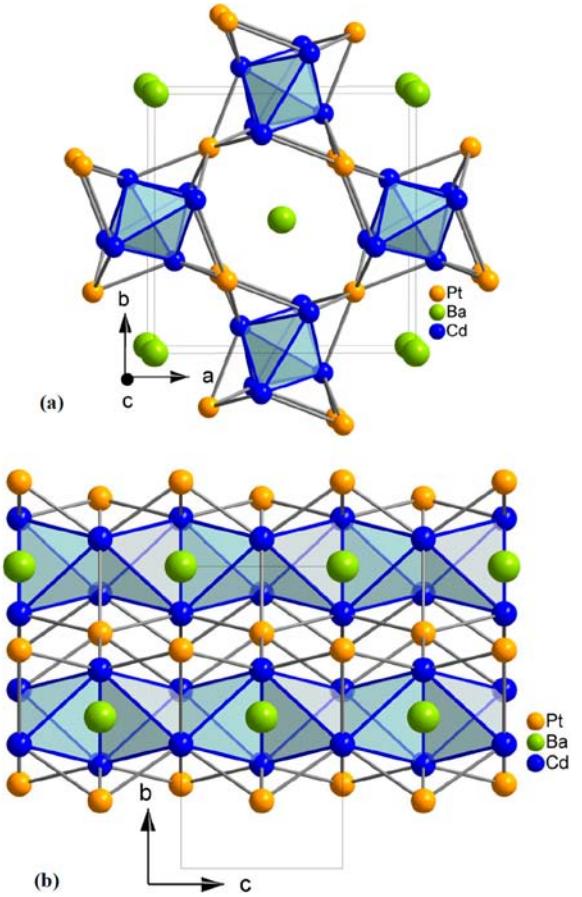

Figure 3. (a) ∼001 view of the $(Sr,Ba)Cd_4Pt_2$ structure. Chains of edge-sharing Cd_4 tetrahedra (blue) along c with their outer edges capped by shared Pt atoms. Sr or Ba cations fill the cavities. (b) ∼100 view of edge-shared Cd_4 tetrahedra condensed into chains along c and further interconnected by six-bonded Pt.

Electronic Structure and Chemical Bonding. *$Ca_6Pt_8Cd_{16}$*. Figure 4 shows the individual electronic densities of states (DOS) (Figure 4a), pDOS for the elements by orbital type according to LMTO-ASA calculations (Figure 4b−d), and COHP data for the nearest neighbor interactions (Figure 4e). The corresponding results for $BaPt_2Cd_4$ appear in Figure 5. Band results for $Ca_6Pt_6Cd_{16}$ indicate some substantial interactions. The expected major Pt 5d band is in fact about twice as wide as that for Au 5d in its close relative $Na_6Au_7Cd_{16}$

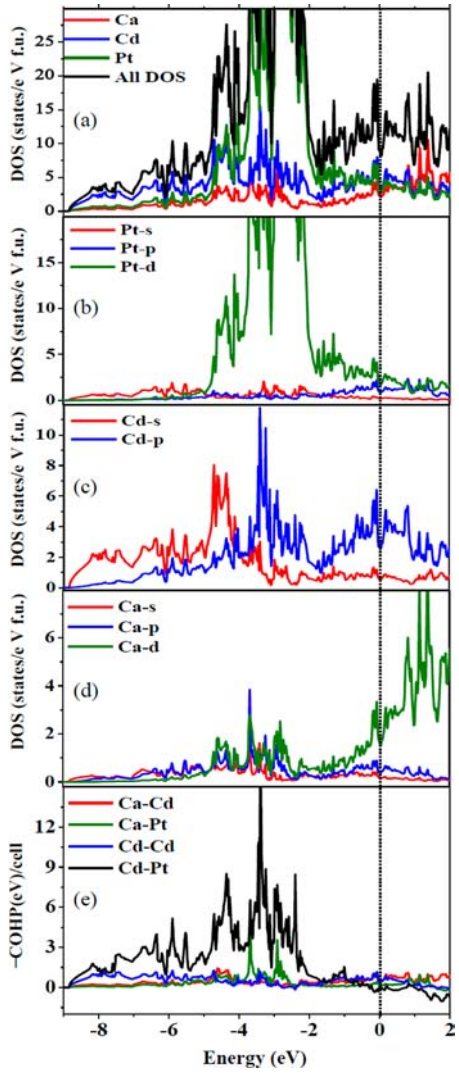

Figure 4. Results of LMTO-ASA calculations for $Ca_6Cd_{16}Pt_8$ cell. (a) Densities of states (DOS) for different atom types. Partial projections of orbital components: (b) Pt 5d, 6s, 6p; (c) Cd 5s, 5p; (d) Ca 4s, 4p, 3d. (e) −COHP values (eV per cell mol) for Pt−Cd (black), Cd−Cd (blue), Ca−Pt (green), and Ca−Cd (red).

dx.doi.org/10.1021/ic302767b | *Inorg. Chem.* 2013, 52, 2697−2704

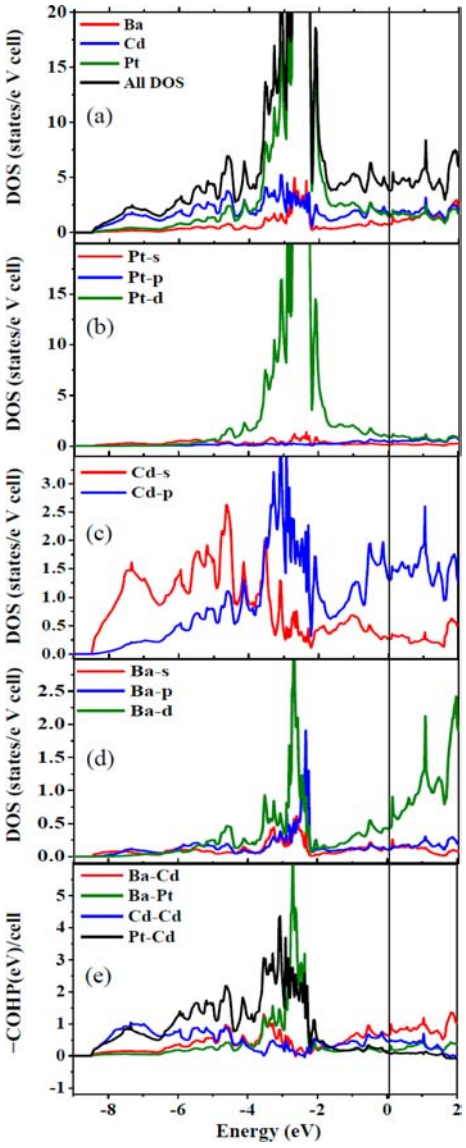

Figure 5. Results of LMTO-ASA calculations for $BaCd_4Pt_2$ cell (Z = 2) considering Cd 4d as core. (a) Density of states (DOS) for different atom types. Partial projections of orbital components: (b) Pt 5d, 6s, 6p; (c) Cd 5s, 5p; (d) Ba 6s, 6p, 5d. (e) COHP values (eV per cell mol) for Pt−Cd (black), Cd−Cd (blue), Ca−Pt (green), and Ca−Cd (red).

with only sodium neighbors.[13] Of course, Pt 5d mixing with Ca 3d is appreciably more consequential than those of Au 5d with Na 3s,p in the gold phase. The Cd 5s and 5p bands are roughly comparable in the two cases. The greater oxidative displacement of some Ca 3d orbital states to above E_F is reminiscent of the still greater fractional oxidation of valence 4d, 5d states of rare-earth metals in related gold phases.[42] The short Pt3−Ca bonds in the octahedra arise from the lower lying Pt 5d states and Ca 3d, as seen in the individual DOS, Figure 4, and correspond to the Ca−Pt3 COHP result in Figures 4 and S5, Supporting Information.

Note should also be made of the appreciable pseudogap at or very near E_F in all of the DOS components for $Ca_6Pt_8Cd_{16}$, Figure 4a (e/a = 1.47 formally). The presence of additional electronic stability at this point is somewhat akin to the special stabilities originally observed in Hume−Rothery phases,[43] in particular, brass-like systems with e/a ratios of about 1.5, although the present ternary intermetallics appear to be line phases with no significant site mixing. This particular pseudogap example can be well explained as what was originally the Jones zone idea or,[44] more contemporarily, in terms of Fermi surface−Brillouin zone interactions at very similar distances.[45] The former can be evaluated in terms of $2K_F = \pi/a(h^2 + k^2 + l^2)^{1/2}$, in which K_F is the radius of the Fermi sphere and h, k, and l are the Miller indices of lattice planes that give rise to particularly large diffraction intensities/emission probabilities. The example of the particularly strong {044} diffraction at a 2Θ angle of about 37.6° in its X-ray powder pattern (see Figure S1a, Supporting Information) yields a Fermi sphere diameter of about 1.294 $Å^{-1}$. This is in turn very close to the center-to-face distance (1.316 $Å^{-1}$) of the Brillouin zones constructed from corresponding zone planes with $|G|^2$ = 32. As the Fermi surface approaches the Brillouin zone polyhedron, electrons on the Fermi surface can spill onto the larger Brillouin zone. Accordingly, the density of electronic states at the Fermi energy drops, resulting in formation of a pseudogap and stabilization of the system. Such Fermi surface−Brillouin zone matching has also been found in different types of quasicrystal approximants.[46]

$BaPt_2Cd_4$. The DOS etc. data for the bridged 1-D chains of Cd tetrahedra in $BaPt_2Cd_4$, Figure 5, show the expected reductions in bonding interactions and in Pt 5d bandwidth relative to the cubic phase but comparable dispersion of the Cd 5s, 5p states remain. (Note the change in DOS amplitude scales in Figure 5 from $f.u.^{-1}$ to $cell^{-1}$.) The Ba 5d DOS and Ba−Pt COHP results appear to be enhanced over those for Ca in the more condensed Ca−Pt−Cd structure. Both phases are predicted to be metallic.

Hamilton Population Analyses. Interatomic distances can be problematic measures of the relative strengths of interatomic interactions even for homoatomic instances, and such means become much more difficult for even semiquantitative comparisons among complex heteroatomic examples. Clearly, bonding analysis of the present nonclassical example is impossible on the basis of distances only, even more so when the numbers of nearest neighbors (the "coordination numbers") become large and the numbers of valence electrons are far below classical octet levels. Fortunately, semiquantitative theoretical bonding analysis programs are available for general experimentalists that provide a suitable level of appreciation and workability if not detailed understanding.

COHP and ICOHP analyses of the LMTO results in Figures 4e and 5e afford useful descriptions of specified pairwise bonding populations as a function of energy and also how well optimized the structure and electron counts are in terms of a match between open bonding levels and E_F. Weighted integrations of the COHP data for each bond type and distance yield the ICOHP "Hamilton populations" (HP) per bond·mol, where after multiplication of each by the frequency of its occurrence per cell gives such total 'bond order' contributions in that solid. Complete ICOHP data for all bond types and distances are listed per mole and per cell for $Ca_6Pt_8Cd_{16}$ and $BaPt_2Cd_4$ in Tables S3 and S5, Supporting Information, whereas the *average* HP values for each pair type over all distances appear in Tables 4 and 5. The averaging over all bonds of a type allows a quicker look at how the bonding is partitioned by atom types, without significant distortions to date.

The largest atom−pair contributions to the total populations or "bonding" in $Ca_6Pt_8Cd_{16}$ are Cd−Pt, ∼52%, and Cd−Cd,

dx.doi.org/10.1021/ic302767b | Inorg. Chem. 2013, 52, 2697−2704

Table 4. Bond Lengths and Average ICOHP Values for Each Bond Type in $Ca_6Pt_8Cd_{16}$

bond	length (Å)	−ICOHP (eV/per bond)	*n*/ cell	−ICOHP (eV/cell)	%
Pt−Cd	2.758(1)−2.967(1)	1.30	224	291.2	52.0
Cd−Cd	3.031(1)−3.244(1)	0.60	192	115.2	20.6
Ca−Pt	2.871(2)−3.884(1)[a]	0.52	144	74.9	13.4
Ca−Cd	3.219(1)−3.221(2)	0.41	192	78.72	14.0

[a]Overly long distance retained for comparison.

Table 5. Bond Lengths and Average ICOHP Values for Each Bond Type in $BaPt_2Cd_4$

bond	length (Å)	−ICOHP (eV/per bond)	*n*/ cell	−ICOHP (eV/cell)	%
Pt−Cd	2.782(1)−2.807(1)	1.48	24	35.52	52.8
Cd−Cd	2.997(1)−3.090(1)	0.72	24	17.28	25.7
Ba−Pt	3.286(1)−3.450(1)	0.65	12	7.80	11.5
Ba−Cd	3.671(1)−3.716(1)	0.28	24	6.72	10.0

~21% (last column). As qualitatively noted from Figure 4, the dominant contribution arises primarily from the overlap between Cd 5s and 5p with Pt 5d orbitals. There are three types of such Cd−Pt bonds (Figure 2a), two for Pt1 atoms bonded to faces of the Cd_8 TS at Cd1 and Cd2, respectively, plus Pt2 bonded to Cd2 atoms in the TSs at 2.806 Å but with only one-third the frequency. These contribute ~26, 18, and 8 to the 52% total per cell, respectively. The strikingly small Ca−Pt3 distances in Pt@Ca_6 octahedra and the larger COHP contribute only 5.9% of the total COHP of the phase and 44% of the total for Ca−Pt because they only occur 25% as frequently as does Ca−Pt1. In terms of atom types, Pt makes the major contributions to the total ICOHP per cell for $Ca_6Pt_8Cd_{16}$, 52% for bonds to Cd and 13.4% for those to Ca. These magnitudes include significant relativistic contributions to the Pt bonding (and for neighboring sixth-period elements in general). For example, the large relativistic-based ICOHP values per bond for the four Pt bonds discussed above (>1.0 eV/bond.mol) are 13−23% larger than without the scalar relativistic corrections, roughly in order of decreasing bond lengths.

According to the COHP data for $BaPt_2Cd_4$, Figure 5e, only the Cd−Pt and Ba−Pt bonding is optimized at E_F. The more substantial bonding contributions to the overall structure again come from Cd−Pt (53%) and Cd−Cd (~26%), Table 5. Pt−Cd bonding arises mostly from separate overlaps of Cd 5s with Pt 6s and of Cd 5p with Pt 5d orbitals, Figure 5e. Our electronic counting methods indicate that the isostructural but seemingly electronically contrasting $ZrFe_4Si_2$ has 44 VE compared with $BaPt_2Cd_4$ with 30 VE, but this is largely an artifact of electron-counting differences for the transition metals.

It is important to note again that both $Ca_6Pt_8Cd_{16}$ ($Sc_6Ir_8Sc_{16}$ type) and gold-deficient $Na_6Au_7Cd_{16}$ are very closely related, crystallizing in the same space group (*Fm*-3*m*) with the same anionic building blocks and very close VEC (44 and 45, respectively). The compositional difference evidently arises because of an appreciable difference in cation−anion bonding. The additional Pt3 in $Ca_6Pt_8Cd_{16}$ stabilizes the Ca octahedra according to the COHP data for Ca−Pt in Figure 4d and 4e and, of course, in the more complex multiphase relationships that define *stability* for $Ca_6Pt_8Cd_{16}$. The comparable Na−Au interaction would not be nearly as significant in $Na_6Cd_{16}Au_8$ (relative to some other Au sink). Not surprising, an attempt to synthesize the $Ca_6Cd_{16}Pt_7$ analog of $Na_6Cd_{16}Au_7$ was unsuccessful too, even in lower yield. Gold analogues of $Ca_6Cd_{16}Pt_8$ or $Ca_6Cd_{16}Pt_7$ could not be formed either, which can be more readily understood in an electronic sense; the e-richer gold would shift E_F by ~0.7 eV into a region of higher lying and largely nonbonding states and away from the pseudogap (Figure 4e).

The π-bonding effect with Ca is naturally lacking with sodium.[13] The ICOHP value for the average Ca−Pt bond (0.52 eV/bond) in $Ca_6Pt_8Cd_{16}$ is much larger than for the Na−Au bond (0.11 eV/bond) in $Na_6Cd_{16}Au_7$, although this comparison does not enter directly into stability discussions. The first larger and partially obscured (green) peak in the COHP data for Ca−Pt at ~−3.7 eV, Figure 4e (see also Figure S5, Supporting Information), corresponds to the Ca 3d−Pt3 5d bonding in the octahedra, the neighboring peak at −2.9 eV coming from the more frequent Ca 3d−Pt1 bonding.

Inverted Isotypic $Er_6Pd_{16}Sb_8$. Comparison of the new $Ca_6Pt_8Cd_{16}$ with other *Fm*-3*m* tetrahedral star examples in the literature revealed a single striking contrast in the recently reported $Er_6Pd_{16}Sb_8$ (which also forms with other late lanthanide metals).[25] The chemical characteristics of the TS formers (two 32*f* sites) and the elements that bridge between them (24*e*, 4*b*, 4*a*) are now reversed, that is, with Pd_{16} in place of Cd_{16} and Sb_8 instead of Pt_8 and hence all of the other chemistry that these types imply. However, the collective elements in the two compounds—$Ca_6Cd_{16}Pt_8$ and $Er_6Pd_{16}Sb_8$—are not so far apart in total valence electron counts, amounting at first impression to a 14e per f.u. increase. However, a perceptive theoretical prediction based on experience, that the $5s^2$ states on Sb would be core like,[47] brings the valence electron count difference down to virtually nothing, −2. Thus, we are left with more indirect comparisons and contrasts for the two phases. The principal features appear to be (a) the greater magnitudes of relativistic corrections for sixth-period element (Pt) versus the corresponding fifth-period transition metal (Pd), (b) relative sizes of metal atoms and distortions these may generate along with individual differences in their bonding orbital properties, and (c) comparisons and contrasts in chemical characteristics between the late transition and early s−p elements, etc., for fifth- and sixth-period systems about which little general or overall chemistry is known. The equivalent positions occupied by Cd versus Pd in these two compounds are a good example.

Comparisons of bonding and structural details for these contrasts seem most useful, whereas we are well short of being able to explain or compare their thermodynamic stabilities in terms of competitive phases. The LMTO and COHP outcomes (per f.u.) for each bond type in $Er_6Pd_{16}Sb_8$ are given in Figure 6 per bond type and per cell for comparison with those for $Ca_6Cd_{16}Pt_8$ in Figure 4. An initial Sb DOS calculation confirmed the expectation of narrow $5s^2$ states (around −14 eV), and conversion of these to core levels led to the results in Figure 6b. The low-lying double peaks for Sb arise from Sb p interactions with Er 6s (~−6 eV) and with mostly Er 5d (~−4 eV), respectively. The broad and dominant Pd 4d states are

dx.doi.org/10.1021/ic302767b | Inorg. Chem. 2013, 52, 2697−2704

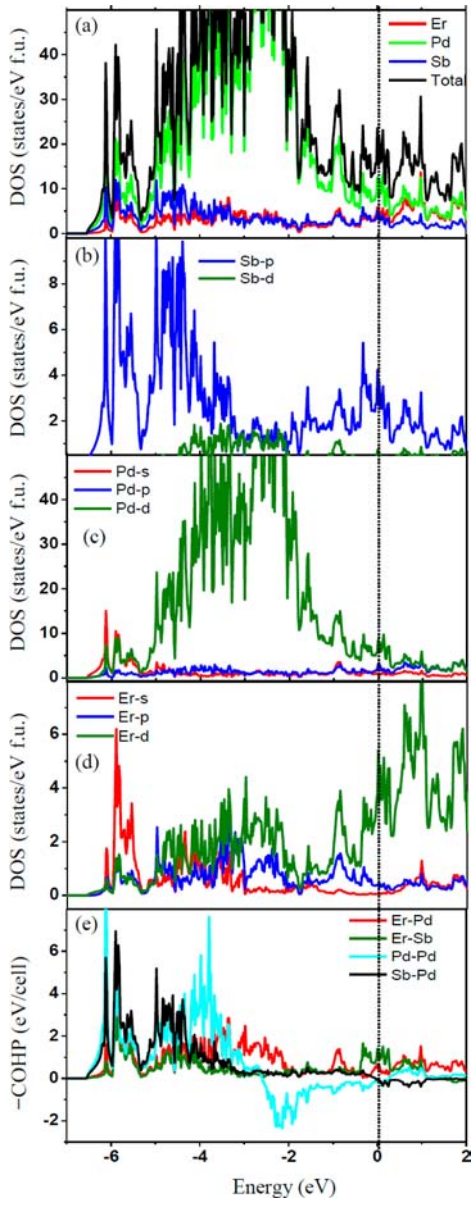

Figure 6. Results of LMTO-ASA calculations for $Er_6Pd_{16}Sb_8$ cell. (a) Densities of states (DOS) for different atom types. Partial projections of orbital components: (b) Sb 5p, 5d; (c) Pd 5s, 5p, 4d; (d) Er 6s, 6p, 5d. (e) COHP values (eV per cell mol).

strongly self-bonded within the TSs in the lower regions as well as with Er 5d around −3 eV. The Sb−Pd COHP is also large around −5 eV, as it is in the parallel yet reversed Pt−Cd COHP in $Ca_6Cd_{16}Pt_8$, Figure 4e. An apparent trend at this point is that the elements with valence d states achieve more/better bonding in the 32*f* TS positions (Pd) than as bridges between the TS in 24*e* (Pt), etc., as it occurs in the inverse arrangement in $Ca_6Cd_{16}Pt_8$. However, this difference is mainly directed by the stoichiometry, with a doubling of the fraction of the d element in the Pd member.

The corresponding Hamilton populations (ICOHP) calculated from the COHP data for $Er_6Pd_{16}Sb_8$ are presented in Table 6 for each bond type and per cell, whereas data for all individual bonds are similarly presented in Table S6, Supporting Information. The HP sums for the most frequent and 'strongest' bond type are found to have dropped from 52% to 42% of the total per cell between $Ca_6Cd_{16}Pt_8$ and $Er_6Pd_{16}Sb_8$

Table 6. Bond Lengths and Average ICOHP Values for Each Bond Type in $Er_6Pd_{16}Sb_8$

bond	length (Å)	−ICOHP (eV/per bond)	*n*/ cell	−ICOHP (eV/cell)	%
Sb−Pd	2.665−2.875	1.13	224	253.12	41.9
Pd−Pd	2.940−3.101	0.66	192	126.72	20.9
Er−Sb	2.925−3.600	0.56	144	80.64	13.3
Er−Pd	3.002−3.156	0.75	192	144.0	23.8

for what are Pt−Cd versus Sb−Pd interactions (with twice the number of d elements in the second), respectively (Tables 4 and 6). Strictly speaking, such comparisons are a bit of 'apples versus oranges', but consistencies throughout suggest some believable trends are present. Increases in ICOHP magnitudes when relativistic corrections are included would, for example, be expected to be less for Pd that for Pt, and they uniformly are 0−11% for the Pd data compared with 11−23% of the total per bond for Pt. Complications with these ICOHP comparisons are the different distributions of the elements in the two phases, e.g., Cd−Cd versus Pd−Pd data for the second bond type for which the Pd−Pd result is a little larger (and the bond distances less). Similarly, the third bond type sets Ca−Pt off against Er−Sb, and the HP results for the latter are only slightly smaller, Er presumably being the more strongly bound cation. However, the last bond types are really not comparable; Ca−Cd HP data are only a little over 50% as large as for Er−Pd, and the bond lengths in the latter are up to 0.20 Å shorter.

In spite of this, the Pd−Sb ICOHP results per bond·mol are 19% less than the comparable data for Cd−Pt (Table 6 versus 4). A distinctively smaller relativistic correction term for Pd appears to be the major source, as might be expected, the "off−on" relativistic corrections in the ICOHP calculations in the former being very small. There are otherwise only small semiquantitative differences between the results in Figures 4 and 6 and Tables 4 and 6: some gain in heteroatomic bonding on changing from Ca to Er and loss of the 5s bonding going from Cd to Sb. More semiquantitative analyses with ICOHP data (above) support these two generalizations. Again, these comparisons do not take into account any differences in competitive alternative phases that define stability, so these comparisons are thermodynamically "off scale". Nonetheless, all three of the very similar network structures are special; by far the largest HP values per bond in each come from the A_8−B_{16} interactions and the next from B_{16}−B_{16} bonds.

Viewpoint. The supposedly simple tasks of looking for Pt or Pd analogues of a recent result with neighboring gold and the diversity of problems encountered remind us that there are not only many factors that determine the matter of stability or not but far more possibilities for products that we can know or imagine. The major determining factor is of course the stabilities of alternate phases, which we generally do not know or think about when a new synthesis target is formed but which we find instead when a well-imagined target or guess does not appear. Experimentation in equilibrium systems generally does not give us any look at what was the second best product, baring a simple composition change. The variety of unimaginable possibilities is in many cases the major handicap when we explore the wilderness, but these can also be

dx.doi.org/10.1021/ic302767b | *Inorg. Chem.* 2013, 52, 2697−2704

the most striking rewards and how many other element combinations will yield a second $A_xB_yC_z$ mountain?

■ ASSOCIATED CONTENT

Supporting Information

Tables of anisotropic displacement parameters for and bond distances in $Ca_6Pt_8Cd_{16}$, $SrPt_2Cd_4$, and $BaPt_2Cd_4$; observed and calculated X-ray powder diffraction data for $Ca_6Pt_8Cd_{16}$, $BaPt_2Cd_4$, and $Er_6Pd_{16}Sb_8$; nearest neighbor figures, cif files. This material is available free of charge via the Internet at http://pubs.acs.org.

■ AUTHOR INFORMATION

Corresponding Author

*E-mail: jcorbett@iastate.edu.

Present Address

[†]Department of Chemical Education, Sriwijaya University, Inderalaya, South Sumatra, Indonesia.

Notes

The authors declare no competing financial interest.

■ ACKNOWLEDGMENTS

F.G. acknowledges the support of the Fulbright Scholar Program. We thank Dr. Olga Zhak of the University of Liviv, Ukraine for the diffraction data set for $Er_6Pd_{16}Sb_8$. This research was supported by the Office of the Basic Energy Sciences, Materials Sciences Division, U.S. Department of Energy (DOE). Ames Laboratory is operated for DOE by Iowa State University under contract no. DE-AC02-07CH11358.

■ REFERENCES

(1) Corbett, J. D. In *Chemistry, Structure and Bonding of Zintl Phases and Ions*; Kauzlarich, S. M., Ed.; VCH Publishers: New York, 1996; Chapter 4

(2) Corbett, J. D. *Angew. Chem., Int. Ed.* **2000**, *39*, 670.

(3) Liu, S. F.; Corbett, J. D. *Inorg. Chem.* **2004**, *43*, 4988.

(4) Li, B.; Corbett, J. D. *Inorg. Chem.* **2005**, *44*, 6515.

(5) Li, B.; Corbett, J. D. *J. Am. Chem. Soc.* **2006**, *128*, 12392.

(6) Li, B.; Corbett, J. D. *Inorg. Chem.* **2007**, *46*, 6022.

(7) Dai, J. -C; Corbett, J. D. *Inorg. Chem.* **2007**, *46*, 4592.

(8) Lin, Q.; Corbett, J. D. *Inorg. Chem.* **2008**, *47*, 7651.

(9) Li, B.; Kim, S.-J.; Miller, G. J.; Corbett, J. D. *Inorg. Chem.* **2009**, *48*, 6573.

(10) Smetana, V.; Corbett, J. D.; Miller, G. J. *Inorg. Chem.* **2012**, *51*, 1695.

(11) Smetana, V.; Miller, G. J.; Corbett, J. D. *Inorg. Chem.* **2012**, *51*, 7711.

(12) Lin, Q.; Corbett, J. D. *Inorg. Chem.* **2011**, *50*, 11091.

(13) Samal, S. L.; Corbett, J. D. *Inorg. Chem.* **2011**, *50*, 7033.

(14) Samal, S. L.; Lin, Q.; Corbett, J. D. *Inorg. Chem.* **2012**, *51*, 9395.

(15) Gupta, S.; Corbett, J. D. *Inorg. Chem.* **2012**, *51*, 2247.

(16) Hoffmann, R. D.; Poettgen, Landrum, G. A.; R.; Dronskowski, R.; Kuennen, B.; Kotzyba, G. *Z. Anorg. Allg. Chem.* **1999**, *625*, 789.

(17) Samal, S. L.; Corbett, J. D. *Z. Anorg. Allg. Chem.* **2012**, *638*, 1963.

(18) Muts, I. R.; Zaremba, V. I.; Rodewald, U. C.; Hermes, W.; Poettgen, R. *Z. Anorg. Allg. Chem.* **2007**, *633*, 2725.

(19) Gritner, K. D.; Schuster, H. U. *Z. Anorg. Allg. Chem.* **1994**, *620*, 1151.

(20) Palasyuk, A.; Corbett, J. D. *Z. Anorg. Allg. Chem.* **2007**, *633*, 2563.

(21) Stojanovic, M.; Latturner, S. E. *J. Solid State Chem.* **2007**, *180*, 907.

(22) Tappe, F.; Pöttgen, R. *Z. Naturforsch.* **2009**, *64b*, 184.

(23) Schappacher, F. M.; Rodewald, U. C.; Pöttgen, R. *Z. Naturforsch.* **2008**, *63b*, 1127.

(24) Corbett, J. D. *Inorg. Chem.* **2010**, *49*, 13.

(25) Zelinska, M.; Oryshchyn, S.; Zhak, O.; Pivan, J. Y.; Potel, M.; Tougait, O.; Noel, H.; Kaczorowski, D. *J. Solid State Chem.* **2010**, *183*, 2121.

(26) Samal, S. L.; Corbett, J. D. Unpublished results.

(27) Baelz, U.; Schubert, K. *J. Less-Common Met.* **1969**, *19*, 300.

(28) *WinXPow 2.10*; Stoe&Cie GmbH: Darmstadt, Germany, 2004.

(29) *SMART*; Bruker AXS, Inc.: Madison, WI, 1996.

(30) Blessing, R. H. *Acta Crystallogr.* **1995**, *A51*, 33.

(31) *SHELXTL*; Bruker AXS, Inc.: Madison, WI, 2000.

(32) Krier, G.; Jepsen, O.; Burkhardt, A.; Andersen, O. K. *TBLMTO-ASA Program*, version 4.7; Max-Planck-Institut für Festkörperforschung: Stuttgart, Germany, 1995.

(33) Jepsen, O.; Andersen, O. K. *Z. Phys. B* **1995**, *97*, 35.

(34) Dronskowski, R.; Blöchl, P. E. *J. Phys. Chem.* **1993**, *97*, 8617.

(35) Chabot, B.; Cenzual, K.; Parthe, E. *Acta Crystallogr., Sect. B* **1980**, *36*, 7.

(36) Florio, J. B.; Rundle, R. E.; Snow, A. I. *Acta Crystallogr.* **1952**, *5*, 449.

(37) Bergman, G.; Waugh, J. L. T. *Acta Crystallogr.* **1956**, *9*, 214.

(38) Häussermann, U.; Svensson, C.; Lidin, S. *J. Am. Chem. Soc.* **1998**, *120*, 3867.

(39) Kaskel, S.; Dong, Z.-C.; Klem, M. T.; Corbett, J. D. *Inorg. Chem.* **2003**, *42*, 1835.

(40) Gulo, F.; Samal, S. L.; Lin, Q.; Corbett, J. D. Unpublished work.

(41) Yarmolyuk, Y. P.; Lysenko, L. A.; Gladyshevskii, E. I. *Dopov. Akad. Nauk Ukr. RSR, Ser. A* **1975**, 279.

(42) Chai, P.; Corbett, J. D. *Inorg. Chem.* **2012**, *51*, 3548.

(43) Hume-Rothery, W.; Raynor, G. V. *The Structure of Metals and Alloys*, 4th ed.; Institute of Metals: London, 1962.

(44) Jones, H. *Proc. R. Soc. London, Ser. A* **1934**, *144*, 225.

(45) Mizutani, U. In *The Science of Complex Alloy Phases*; Massalski, T. B., Turchi, P. E. A., Eds.; The Minerals, Metals & Materials Society: Warrendale, PA, 2005; p 1.

(46) Lin, Q.; Corbett, J. D. *Inorg. Chem.* **2011**, *50*, 11091.

(47) Miller, G. J. *Private communication*, 2012.